THE JOURNAL OF PHYSICAL CHEMISTRY C

Article

Cite This: J. Phys. Chem. C 2018, 122, 27350−27359

pubs.acs.org/JPCC

Confinement Effects in Protonation Reactions Catalyzed by Zeolites with Large Void Structures

M. Fernanda Zalazar,*[,†,‡] Néstor Damián Cabral,[†] Gonzalo D. Romero Ojeda,[†] Clara Iris Aymará Alegre,[†,‡] and Nélida M. Peruchena[†,‡]

[†]Laboratorio de Estructura Molecular y Propiedades (LEMYP), Facultad de Ciencias Exactas, Naturales y Agrimensura, Universidad Nacional del Nordeste (UNNE), Avenida Libertad 5460, 3400 Corrientes, Argentina

[‡]Instituto de Química Básica y Aplicada del Nordeste Argentino, IQUIBA-NEA, CONICET-UNNE, Avenida Libertad 5460, 3400 Corrientes, Argentina

Supporting Information

ABSTRACT: In the present work, we studied the protonation reaction of styrene inside the cavity of acidic H-Y zeolite. Density functional theory calculation using M06-2X functional and analysis of quantum theory of atoms in molecules are used to investigate the confinement effects of zeolite framework on species involved on the reaction. A detailed analysis of the topology of the electron density of interactions among reactants, transition state, and intermediate products with the cavity of H-Y zeolite is performed, extracting conclusions about adsorption, catalysis, and confinement effects. Identification and quantification of host−guest interactions between zeolite framework and styryl cation support the larger contribution of weak closed-shell interactions in stabilization of the formed carbenium ion. Our results clearly show that reaction energies for all formed species inside a zeolite with large void structure are also significantly governed by the confinement effects related to weak host−guest interactions. In other words, zeolite confinement effect is a crucial factor that may affect the catalytic activity even on zeolites with large pore size and void structure as H-Y.

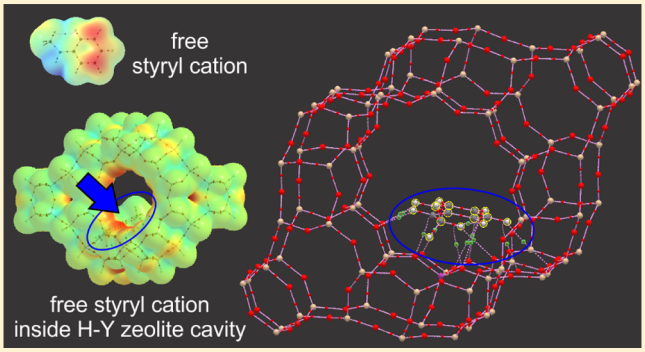

1. INTRODUCTION

Zeolites are microporous solids widely used in fine chemistry,[1] oil refining, and petrochemistry as heterogeneous catalysts.[2] They possess pores, cavities, and channels with well-defined molecular dimensions that provide a selective environment acting as a nanoreactor.[3] There are two main factors that affect the stabilities of confined species in acidic zeolite pore, i.e., Brønsted acid strength and pore confinement effect.[4] The interactions between the zeolite framework and the confined molecules play a key role in adsorption and the catalytic properties of zeolites by stabilizing adsorbed molecules, intermediates, and transition states (TSs). This effect is known as confinement effect, and because of it, zeolites can be described as solid solvents.[5,6]

Confinement and solvation by van der Waals (vdW) forces confer remarkable diversity to zeolites, in spite of their structural rigidity and their common aluminosilicate composition.[7] The confinement effects on zeolites have received wide attention over the last years, and numerous studies on the role of confinement have been conducted by using different experimental and theoretical methodologies.[4,7−19] Although many research works have been done in this area, a clear chemical picture about the pore confinement has not been established.

Buurmans et al. studied the reaction of the oligomerization of 4-fluorostyrene on H-ZSM-5 and H-Y and suggested using geometrical bond distances less than 3.2 Å as a criterion of intermolecular contact that numerous weak contacts are involved in the stabilization of various bulky hydrocarbon species formed in zeolitic voids.[20] Recently, Ristanović et al. have studied proton-transfer processes within a zeolite crystal and discussed that understanding the synergy between the numerous physicochemical processes taking place inside zeolites demands for fundamental insights into the host−guest interactions, where porosity, guest mobility, and solvent effects can strongly interfere with Brønsted acid-catalyzed processes.[21]

In previous studies of chemical reactions of interest in the zeolite chemistry, we demonstrated the usefulness of quantum theory of atoms in molecules (QTAIMs) analysis and the relevance of the information that can be obtained through the analysis of electron density distribution.[22−25] One of the advantages of the QTAIM methodology over other global measures of the interaction energy is that it allows one to

Received: July 30, 2018
Revised: November 12, 2018
Published: November 14, 2018

DOI: 10.1021/acs.jpcc.8b07357
J. Phys. Chem. C 2018, 122, 27350−27359

decompose the interaction energy in contributions by an atom or a group of atoms, and because of which it was used in the analysis, design, and optimization of ligand molecules in the ligand/receptor recognition process.[26] Similar analysis could be applied in the study of adsorbate−catalyst interactions, which makes it particularly useful for these catalytic systems where several interactions are found.

In a very recent study, we have shown that interactions related to the confinement effects and the reaction itself (adsorption, coadsorption, bond-breaking, and bond-forming processes) can be discriminated, to discriminate the relative contributions of the degree of confinement to the reaction energies for two zeolite catalysts with small and medium pore voids.[27] According to this study, for adsorbed and coadsorbed complexes and intermediate species, stabilization in the smaller zeolite cavity is dominated by the confinement effect of the catalyst on the reactant species; however, for transition state, the stability is achieved due to the stabilizing effect of the surrounding zeolite framework on the formed carbocationic species (CH_3^+) and it is of greater importance the higher available space to guarantee the proper orientation of fragments or species involved in the formation of transition state.

However, it should be emphasized that each zeolite framework contains diverse solvating environments. H-FAU (acid faujasite) is considered a large-pore zeolite with large supercages,[28] so it may be thought that the effects of confinement do not influence or are not of significant importance in the initial steps of the reaction when small bulky intermediates are being formed. However, we suggest that weak interactions are of paramount importance even on zeolites with large pore size and void structure. New insights based on electron density analysis could help to answer the question about what is the influence of lattice atoms on stabilizing the intermediates when a zeolite with a large pore structure is considered. An in-depth understanding of the species involved on the mechanism, identifying the electronic properties of the transition states, will also allow to identify relevant properties that the catalyst should fulfill and that serve as a complement in the design of catalysts to guide the reactivity-selectivity.

Styrene is an important monomer that is industrially applied for the synthesis of plastics and rubbers.[29] For polymerization processes of styrene on zeolites, the initial step of the reaction is the generation of a charged carbon moiety and the formation of carbocation species; then, dimerization and subsequent protonation are the chemical reactions for the synthesis of those macromolecules.[30] Further insights into elementary reactions as protonation of styrene and formation of carbocation species are of interest for several reaction mechanisms involving dimerization of styrene.[31] It is not only the extreme acidity of zeolites but also other special properties of the internal voids that make these solids very appropriate to stabilize positively charged reaction intermediates.[32]

In the present work, we further investigate the solvation of the H-Y zeolite framework on species involved in the protonation reaction of styrene. Molecular electrostatic potential (MEP) maps and QTAIM[33,34] analysis are used to study the stability of intermediates of reaction of styrene inside the cavity of H-Y zeolite. A detailed analysis of the topology of the electron density of interactions among reactants, TS, and intermediate products with the cavity of zeolites is performed, extracting conclusions about adsorption, catalysis, and confinement effects. We try to show that the stabilization energies of all formed species during the reaction inside a zeolite with large pore and void structure are also significantly governed by confinement effects related to weak host−guest interactions besides the acid strength. The understanding and the characterization of host−guest interactions in zeolites are essential to explain the observed reactivity in these catalytic processes.

2. METHOD AND CALCULATION DETAILS

Coordinates of the FAU zeolite framework were obtained from the International Zeolite Association online database.[35] To cover the confinement effect from the zeolite framework, the H-Y zeolite catalyst has been modeled by a 84T (T = Si and Al tetrahedral sites) cluster model cut out from the zeolite crystal structure. The dangling bonds that connect the cluster with the rest of the solid have been saturated with hydrogen atoms at a bond length of 1.47 Å from the silicon atoms and orientated toward the corresponding Si−O bonds of the zeolite. To introduce acidic center, we replaced one of the symmetry-equivalent Si atoms by an Al atom, where the active site was positioned at the Si1−O4(H)−Al1 site.[36] The net negative charge of the lattice due to the substitution of one silicon atom by an aluminum atom was compensated by a proton on a bridging oxygen center of the type Si−O−Al. The resulting 84T zeolite model has a total of 289 atoms, with an overall composition of $[O_{3/2}SiH]_{72}[SiO_2]_{10}[O_{3/2}Si(OH)AlO_{3/2}]$. This extended cluster includes two supercages connected via a 12-membered ring window with a free aperture of 7.4 × 7.4 Å. Therefore, local effects (interaction of adsorbate with the Brønsted and Lewis sites) and nonlocal effects (van der Waals interactions with the zeolite cavity or confinement effects) are taken into account.

Because the system is computationally demanding, we used a combined theoretical model, namely, ONIOM [M06-2X/6-31+G(d,p):PM6], to predict the geometries of all intermediates and transition states. Previous studies showed that the density functional theory using the M06-2X[37,38] functional provided quite good results compared to functionals without dispersion energy terms for studying the interaction of organic molecules inside the zeolite pores.[27,38−44] Additionally, the semiempirical PM6[45] method has been used in ONIOM schemes for the study of reactions on zeolites.[46−48] A 10T region (including the acid site) and the organic molecules were considered as the high-level layer, whereas the remainder of the system were considered as the low-level layer. The resulting ONIOM model for isolated H-Y is labeled as 10T/84T. During geometry optimization, the reactant molecules and atoms located in the 10T high-level layer of zeolite model were allowed to fully relax, whereas the remaining atoms of the 84T zeolite model in the low-level layer were frozen at their optimized crystallographic position. All stationary points were characterized by calculating the Hessian matrix and analyzing the vibrational normal modes.

To obtain more accurate interaction energies, single point (SP) calculations with the M06-2X[37,38] density functional and the 6-31++G(d,p) basis set were carried out, using the optimized geometries produced by the ONIOM calculations. All calculations were performed with the Gaussian 09 program.[49]

We discuss the nature of host−guest interactions by means of a topological analysis of the electron charge density

DOI: 10.1021/acs.jpcc.8b07357
J. Phys. Chem. C 2018, 122, 27350−27359

distribution in the framework of atoms in molecules theory (QTAIM).[33,34,50] The topological analysis of the electron density, $\rho(r)$, and its Laplacian function, $\nabla^2\rho(r)$, constitute a powerful tool to investigate the nature of the chemical bonds.[33] According to Bader theory, the presence of a bond path (BP) is a universal indicator of the existence of a bonding interaction.[51] Total electron densities were obtained at M06-2X/6-31++G(d,p) level by the Gaussian program. The bond and atomic properties were calculated using the AIMAll software.[52] The maps of molecular electrostatic potential (MEP) were calculated and drawn with the AIMAll program using a 0.001 au electron density isosurface.

Bader's net atomic charges were determined on selected atoms. The accuracy of the integration over the atomic basin (Ω) was assessed by the magnitude of a function $L(\Omega)$, which, in all cases, is less than 10^{-5} au for H atoms and 10^{-4} au for other atoms. We have employed a similar QTAIM analysis in our previous works on the reaction of alkenes over acidic zeolite.[22,23,25,27]

Additionally, the reduced density gradient (RDG), [defined as $s = 1/(2(3\pi^2)^{1/3})|\nabla\rho(r)|/(\rho(r)^{4/3})$], together with the electron density, was used to reveal noncovalent interactions.[53] Intramolecular interactions were omitted for the calculated RDG function to elucidate intermolecular noncovalent interactions between the adsorbates and the zeolite frameworks. The functions RDG and sign(λ_2)ρ (the sign of the second largest eigenvalue of the electron density Hessian matrix multiplied by the electron density) were calculated using Multiwfn software.[54] Previous studies showed that the gradient isosurfaces provide a rich visualization of noncovalent interactions between organic molecules inside the zeolite pores.[55,56]

3. RESULTS AND DISCUSSION

Figure 1 displays the most stable structures and their relative energies along the reaction coordinate calculated at SP M06-2X/6-31++G(d,p) level. SP energies decrease by about 9−11 kcal mol^{-1} when comparing energies using the ONIOM methodology. The transition states explored are carbenium ion-like. Next, we briefly discuss the peculiarities of the mechanism.

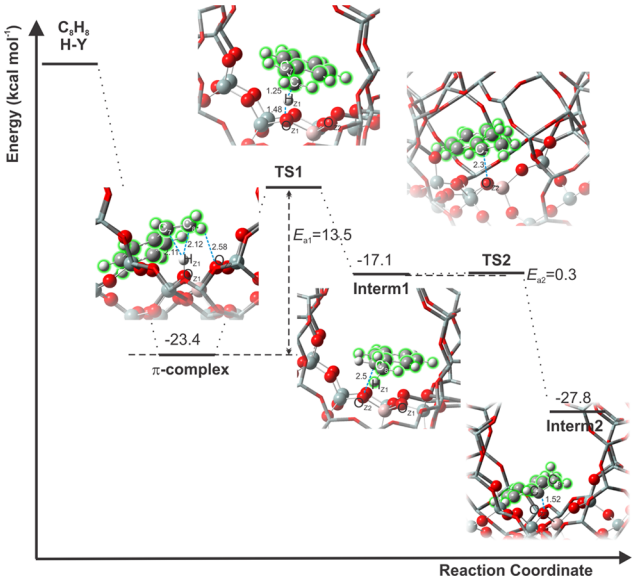

Figure 1. Energy profiles for the protonation reaction of styrene over H-Y zeolite at SP M06-2X/6-31++G(d,p) level.

The initial step starts with the physisorption of a styrene molecule on the Brønsted acid site (BAS) of the H-Y zeolite and a π-complex is formed (Figure 1), where the acidic proton of the BAS, H_{Z1}, is about halfway between the C_7 and C_8 atoms of the vinyl double bond of styrene (2.11 and 2.12 Å). At the TS1, the acidic proton has protonated the styrene molecule and the C_7-C_8 double bond on the vinyl group of styrene is cleaved leading to the formation of a secondary $C_8H_9^+$ carbocation that is stabilized by the adjacent aromatic ring, the corresponding energy barrier is 13.5 kcal mol^{-1}.

Further progress of the reaction implies the formation of a methylphenyl carbenium ion as a stable intermediate (interm1 or styryl cation), where an hybridization change from C(sp^2) to C(sp^3) is observed. The free carbenium ion is 17.1 kcal mol^{-1} lower in energy than gas-phase reactants, and about 6.3 kcal mol^{-1} less stable than the adsorbed π-complex. Then, the positive charge on the electron-deficient carbon center (C_7) of carbenium ion interacts with the oxygen (O_{Z2}) of the Al−O−Si bridge, giving rise to the second transition state (TS2), although the energy barrier is very low (imaginary frequency is associated with the $C_7\cdots O_{Z2}$ bond formation). The lifetime of carbenium ion depends on the barriers separating the carbenium ion from the alkoxide and the physisorbed species.[57]

Subsequent stabilization results in the formation of C_7-O_{Z2} bond and consequently, the alkoxy intermediate bound to the catalyst (interm2 or 1-phenyl-ethoxide). The interm2 is 4.4 kcal mol^{-1} lower in energy than π-complex and is found to be stabilized. That is, the reaction energies show that the alkoxide is more stable than the π-complex by about 4.4 kcal mol^{-1} and the interm1 by about 10.7 kcal mol^{-1}. The $C_7\cdots O_{Z2}$ distance decreases from 2.5 Å in interm1 to 2.3 Å in TS2 and finally 1.52 Å in interm2, reflecting the C−O bond formation. The intermediate ion could deprotonate rapidly, regenerating the BAS of the zeolite, or further dimerization/oligomerization also leads to the formation of bulky species.

Our energy results display lower values than those reported for π-complex and intermediates by other authors at ONIOM M06-2X/6-31G(d):AM1 level with a 8T/84T cluster model.[36] The calculated energy for styrene adsorption in H-Y at SP M06-2X/6-31++G(d,p) level is −1.2 kcal mol^{-1}, lower than that the calculated energy value of −22.2 kcal mol^{-1} informed by Fang et al.[36] reflecting a higher interaction of the adsorbate with the catalyst. No experimental data for styrene adsorption on H-Y or activation energies are found in the literature. Also, interm1 (−17.1 vs −12.2 kcal mol^{-1}) and interm2 (−27.8 vs −19.5 kcal mol^{-1}) are more stable than the ones informed by Fang et al. Summing up, SP calculations decrease the energies by about 9−11 kcal mol^{-1} and improve the study of hydrogen-bonding and van der Waals (vdW) interactions. For the initial carbocation, calculations using a periodic model and the Perdew−Burke−Ernzerhof functional showed energy values of −3 and of 21.2 kcal mol^{-1}, respectively, with correction by vdW interactions.[20]

3.1. Molecular Electrostatic Potential. A previous work showed that the use of topological analysis based on electron density distribution in combination with molecular electrostatic potential (MEP) maps provides valuable information about the steric volume, shape, and the electronic properties of zeolite framework providing a representative measurement of the overall molecular charge distribution.[27]

DOI: 10.1021/acs.jpcc.8b07357
J. Phys. Chem. C 2018, 122, 27350−27359

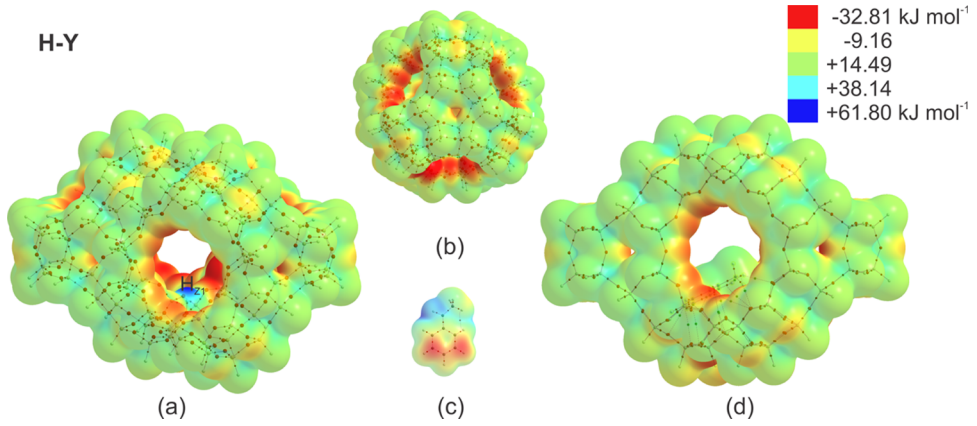

Figure 2. Molecular electrostatic potential on the 0.001 au electron density isosurface for (a) and (b) two views of H-Y zeolite, (c) $C_8H_9^+$ isolated carbenium ion of styrene, and (d) interm1 confined in H-Y zeolite. The red and blue areas indicate negative and positive regions, respectively, varying between −32.81 and +61.80 kcal mol^{-1}. The molecular graphs of $\rho(r)$ are also observed.

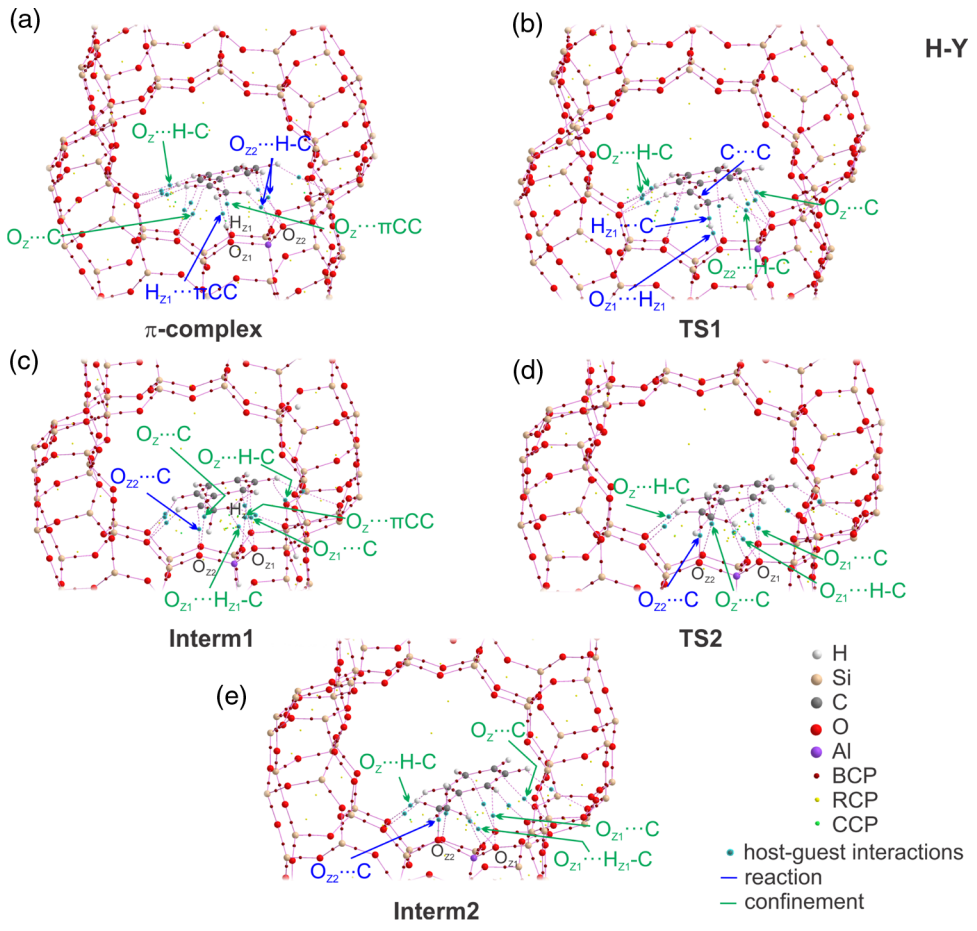

Figure 3. Molecular graphs for the most stable species along the reaction coordinate: (a) π-complex, (b) TS1 for protonation of styrene by BAS, (c) intermediate that involved a carbenium ion (d) TS2, and (e) intermediate that involved an alkoxide bounded to catalyst. The large circles correspond to attractors attributed to nuclei, the lines connecting the nuclei are the bond paths, and the small red circles on them are the bond critical points (BCPs). Terminal H atoms of the Si−H bonds in the zeolite were omitted for clarity.

Figure 2 shows tridimensional MEP maps of the isolated zeolite (a and b), isolated methylphenyl carbenium ion (c), and the methylphenyl carbenium ion within H-Y (d) at the van der Waals surface, representing electrostatic potentials superimposed onto a surface of constant electron charge density (0.001 e au^{-3}). The value of the electrostatic potential ranges from −32.81 kcal mol^{-1} (deep red) to +61.80 kcal mol^{-1} (deep blue). For isolated zeolite catalyst, it is clear that the most negative regions (red regions) are localized over the oxygen atoms inside the cavity, where there is high electron density, and the most positive region (blue) is localized over the BAS, where there is low electron density. The high electron density available inside the cavity shows the high availability of sites for interaction with electron-deficient sites in the guest molecule,

DOI: 10.1021/acs.jpcc.8b07357
J. Phys. Chem. C 2018, 122, 27350−27359

Table 1. Bond Distances (Å) and Local Topological Properties (au) of the Electron Charge Density Distribution Calculated at the Position of the Bond Critical Points for Stationary Points Involved in the Reaction of Protonation of Styrene on H-Y Zeolite[a,b]

	n	interaction$_{X\cdots Y}$	$d_{X\cdots Y}$	$\rho(r)$	$\nabla^2\rho(r)$	$H(r)$	$\sum\rho(r)$
π-complex							
adsorption	1	$H_{Z1}\cdots\pi$CC	2.12	0.0249	0.0559	0.0003	0.0249
	2	$O_{Z2}\cdots$H−C	2.58−2.87	0.008−0.006	0.029−0.021	0.0009−0.0009	0.0144
confinement	6	$O_Z\cdots$H−C	2.69−3.22	0.007−0.002	0.023−0.009	0.0008−0.0006	0.0270
	4	$O_Z\cdots$C	3.11−3.27	0.008−0.006	0.027−0.022	0.0008−0.0008	0.0277
	1	$O_Z\cdots\pi$CC	3.29	0.0067	0.0209	0.0007	0.0067
TS1							
bond breaking	1	C···C	1.40	0.3059	−0.8255	−0.3123	0.3059
	1	$O_{Z1}\cdots H_{Z1}$	1.48	0.0827	0.1315	−0.0219	0.0827
bond forming	1	$H_{Z1}\cdots$C	1.25	0.1789	−0.4548	−0.1498	0.1789
confinement	5	$O_Z\cdots$C	3.01−3.29	0.009−0.006	0.035−0.020	0.0013−0.0007	0.0379
	4	$O_Z\cdots$H−C	2.45−2.88	0.010−0.005	0.033−0.019	0.0010−0.0005	0.0281
	2	$O_{Z2}\cdots$H−C	2.45−2.71	0.011−0.007	0.038−0.025	0.0010−0.0008	0.0180
interm1							
stabilization	1	$O_{Z2}\cdots$C	2.50	0.0217	0.0715	0.0005	0.0217
confinement	6	$O_Z\cdots$H−C	2.34−3.27	0.013−0.002	0.042−0.008	0.0009−0.0003	0.0355
	2	$O_Z\cdots$C	3.12−3.15	0.008−0.007	0.026−0.025	0.0009−0.0008	0.0154
	1	$O_Z\cdots\pi$CC	3.28	0.0068	0.0226	0.0008	0.0068
	1	$O_{Z1}\cdots$C	3.07	0.0095	0.0343	0.0013	0.0095
	1	$O_{Z1}\cdots H_{Z1}$−C	2.59	0.0107	0.0411	0.0014	0.0107
TS2							
bond forming	1	$O_{Z2}\cdots$C	2.30	0.0321	0.0934	−0.0009	0.0321
confinement	4	$O_Z\cdots$C	3.26−3.71	0.007−0.003	0.024−0.010	0.0009−0.0006	0.0230
	3	$O_Z\cdots$H−C	2.22−3.07	0.016−0.003	0.053−0.011	0.0009−0.0001	0.0238
	1	$O_{Z1}\cdots$C	3.02	0.0104	0.0377	0.0013	0.0104
	1	$O_{Z1}\cdots$H−C	2.37	0.0133	0.0447	0.0006	0.0133
interm2							
bond forming	1	O_{Z2}−C	1.52	0.1854	−0.1853	−0.2092	0.1854
confinement	4	$O_Z\cdots$H−C	2.15−3.39	0.021−0.002	0.076−0.006	0.0011−0.0005	0.0344
	4	$O_Z\cdots$C	2.27−3.95	0.010−0.002	0.031−0.006	0.0009−0.0004	0.0226
	1	$O_{Z1}\cdots H_{Z1}$−C	2.29	0.0153	0.0510	0.0005	0.0153
	1	$O_{Z1}\cdots$C	3.05	0.0104	0.0372	0.0013	0.0104

[a]Number of interactions [n], bond distances ($d_{X\cdots Y}$), electron density [$\rho(r)$], Laplacian of electron density [$\nabla^2\rho(r)$], total energy density, [$H(r)$], and sum of electron density values [$\sum\rho(r)$], in au. [b]For $n > 1$, the table informs the range (minimal and maximal) of property values.

and MEP could be of particular interest to predict adsorbate−catalyst interaction modes. Furthermore, these interactions can be quantified and discriminated in terms of electron density distribution.

It can be observed that the zeolite cavity is large enough to accommodate the guest molecule, transition species, and intermediates, and the size of the intermediate (Figure 2c) is small in relation to the size of the cavity. In general, the cavities provide the spatial room for the intermediates and transition states generated during the reaction, and for H-Y, a more spacious cavity minimizes steric constraints.

When considering the formation of the intermediate inside the cavity, its charge is stabilized, which is appreciated through the electrostatic potential by the predominance of green color (Figure 2d). It is also observed that a large space of the zeolite cavity remains empty (although the organic molecules are large enough) and then that confinement effects should not be of significant importance in this zeolite or should not be appreciable in relation to other smaller zeolites as H-ZSM-5 or H-β.[27]

The visualization of isosurfaces of reduced density gradient in real space can describe the noncovalent interactions between the organic fragments and the zeolite frameworks. The colored isosurface indicates the strength of the nonbonded interactions present between both molecules (see Figure S1 of the Supporting Information). It can be observed that the space between the styrene and zeolite is filled with green-colored isosurface that illustrates the weak interaction between them, except for the interactions of styrene with the acidic and basic sites (strong interactions). In the next section, we have quantified these interactions and also covalent interactions related to the reaction in terms of the QTAIM methodology.

3.2. Electron Density Analysis. The molecular graphs of electron density for the most stable structures in H-Y are shown in Figure 3. From topological electron density calculations, a large quantity of bond, ring, and cage critical points (CPs) appears. However, only the most meaningful CPs with respect to the catalysis and confinement phenomena are considered and discussed in detail. The bond critical points (BCPs) and the linking bond paths detected between host−guest interactions are highlighted. Table 1 lists the bond distances and the most relevant topological properties of the electron density at the BCP for most stable species: the electron densities [$\rho(r)$], the Laplacian of the electron density [$\nabla^2\rho(r)$], and the total energy density [$H(r)$]. A summary of

DOI: 10.1021/acs.jpcc.8b07357
J. Phys. Chem. C 2018, 122, 27350−27359

the main properties of ring critical points (RCPs) and cage critical points (CCPs) is presented in Table 2.

Table 2. Electron Charge Density Calculated at the Position of the Ring (RCP) and Cage (CCP) Critical Points[a]

		n	$\rho(r)_{min}$	$\rho(r)_{max}$	$\sum\rho(r)$
RCP					
	π-complex	22	0.000011	0.0051	0.097
	TS1	19	0.000003	0.0076	0.080
	interm1	23	0.000001	0.0092	0.097
	TS2	20	0.000002	0.0114	0.088
	interm2	18	0.000002	0.0177	0.096
CCP					
	π-complex	5	0.000431	0.0036	0.011
	TS1	5	0.001289	0.0038	0.014
	interm1	6	0.000624	0.0064	0.026
	TS2	5	0.000666	0.0062	0.020
	interm2	4	0.000538	0.0066	0.013

[a]Number of critical points [n], minimal electron density value [$\rho(r)_{min}$], maximum electron density value [$\rho(r)_{min}$], and sum of electron density values [$\sum\rho(r)$], in au.

Because the use of topological concepts is well documented in the standard literature,[33,34,50] here, we only presented the essential theoretical information that is needed to discuss results. The local topological properties at the BCP can be used to describe the strength of a bond. In general, the larger the magnitudes of $\rho(r)$, $\nabla^2\rho(r)$, and $H(r)$, the stronger the bond. Additionally, the sign of the total energy density, defined as the sum of the potential and kinetic energy densities at a critical point, is an indicator of covalence in chemical interactions.[58−60] Thus, negative $H(r)$ values indicate a significant sharing of electrons.

The overall picture that can be extracted from the results shown in Figure 3 and Table 1 is that several interactions among the aromatic molecule and the oxygen atoms of the zeolitic lattice (host−guest interactions) are observed. It is interesting to highlight that for all species, all interactions involved only a fraction of atoms of zeolite lattice under the organic fragment. That is, only interactions between the nearest atoms in the zeolite and the bottom of styrene molecule are observed. Our previous study using H-β and H-ZSM-5 zeolites showed interactions between the whole molecule and the zeolite wall, showing that the confinement is related to the whole cavity of catalyst.[27]

Analysis derived from the topological properties of the electron density distribution allows to associate each interaction with a particular phenomenon of the process, discriminating adsorption from confinement, as well as bond breaking/bond forming and stabilization.[27] In other words, in this type of catalytic systems, where a large quantity of host−guest interactions are present, the interactions can be rationalized in terms of their relative contribution to the total process.

To make clear the analysis and description of the results, we define three types of oxygen atoms: (i) the oxygen of the Brønsted acid site (O_{Z1}); (ii) the basic oxygen of the Al−O−Si bridge (O_{Z2}); and (iii) the rest of oxygen atoms of zeolite lattice (O_Z). On the basis of electron density analyses, the adsorbate−catalyst system was partitioned in a first subsystem directly related to the reaction itself and involves the interactions between the adsorbate and BAS and O_{Z2} and a second subsystem related to the confinement effects that involves interactions among the organic species and O_Z.

3.2.1. Adsorbed Styrene. At the adsorbed complex, the proton of BAS is practically located at the same distance from both carbon atoms of the vinyl double bond (2.11 and 2.12 Å). However, only a bond critical point between the proton of BAS and the middle point of the vinyl double bond (C_7−C_8) can be found; thus, no individual $H_{Z1}\cdots C$ bonds are found (see Figure 3 and Table 1). This is not an unexpected behavior since adsorption of light alkenes on a small zeolite model showed similar behavior.[25] The topological properties at the BCP for the $H_{Z1}\cdots\pi CC$ interaction show characteristics of closed-shell interactions, and it constitutes a clear indicator of the formation of the π-complex. The same one can be considered as an unusual hydrogen bond (HB) with moderate strength according to their topological properties.[25] Two more $O_{Z2}\cdots H-C$ interactions involving the basic oxygen of the Al−O−Si bridge are found, and we also related these interactions to the adsorption process. The distances range from 2.58 to 2.87 Å, and the $\rho(r)$, $\nabla^2\rho(r)$, and $H(r)$ values are positive.

Figure 2 showed a large electron density inside the cage of H-Y isolated catalyst, suggesting that several more adsorbate−catalyst interactions between the oxygen atoms of zeolite and the guest molecule could be found, and therefore their contribution to the adsorption energy should be considerable.

It can be observed in Figure 3 that numerous interactions with the oxygen atoms of the zeolite walls [denoted as $O_Z\cdots H-C$, $O_Z\cdots C$ and $O_Z\cdots\pi CC$] are found, we related these last ones to the confinement effects. Six $O_Z\cdots H-C$ interactions (between O_Z and the hydrogen atoms of C−H bonds of styrene), four $O_Z\cdots C$ interactions (among O_Z and carbon atoms), and one $O_Z\cdots\pi CC$ interaction (between O_Z and the π-cloud of phenyl group of styrene) are found. Thus, the π-complex is further stabilized by establishing interactions with the zeolite wall. The results of the AIM analysis provided in Table 1 give information about the nature of these interactions.

The interactions related to the confinement effects show large bond distances (where $d_{X\cdots Y}$ ranges from 2.7 to 3.3 Å) and topological characteristics of very weak closed-shell interactions [$\rho(r) < 0.008$ au; $\nabla^2\rho(r)$ and $H(r)$ values are positive]. These results suggest that the confinement effect is important, even higher than the adsorption itself. That is, 61% of ρ_T [calculated as $\sum\rho(r)$] is attributed to the confinement effect, while 39% is related to adsorption (E_{ads} = −23.4 kcal mol^{-1}). Thus, the presence of numerous weak interactions contributes to the stabilization of the adsorbed π-complex, even if the cavity size is large enough in relation to the confined reagent. For benzene coadsorption in H-β and H-ZSM-5 zeolites, it is found that confinement interactions involved very weak interactions with larger distances up to 3.5 and 3.64 Å and, due to the smaller available space, it involved the whole cavity.[27]

If we consider that the strongest interactions of the adsorbate with the surface come from the interactions with the BAS and O_{Z2}, the adsorption energy without taking into account confinement effect can be estimated by about −9.1 kcal mol^{-1}; therefore, the confinement effects inside the cavity play a crucial role even in zeolites with large void structure.

*3.2.2. Transition State (**TS1**).* In the TS1 (Figure 3), the key interactions related to reaction itself are $O_{Z1}\cdots H_{Z1}$ and $C\cdots C$ bond breaking and $H_{Z1}\cdots C$ bond forming (between the proton of BAS and carbon of vinyl moiety). It can be observed that the proton of BAS is dicoordinated $O_{Z1}\cdots H_{Z1}\cdots C$. The $\rho(r)$ value

DOI: 10.1021/acs.jpcc.8b07357
J. Phys. Chem. C 2018, 122, 27350−27359

of $H_{Z1}\cdots C$ is about 2 times higher than the same value in $O_{Z1}\cdots H_{Z1}$, and $\nabla^2\rho(r) > 0$ and $H(r) < 0$, showing that the $O_{Z1}\cdots H_{Z1}$ bond breaking is weaker than $H_{Z1}\cdots C$ bond forming or the proton transfer is more advanced toward intermediate. Bonds with positive values of $\nabla^2\rho(r)$ and small negative values of $H(r)$ at BCP are termed as partially covalent in nature. Interestingly, both interactions show covalent character. In general, the larger the $\rho(r)$ value, the stronger the bond.[33,34] In addition, the C···C bond breaking shows smaller values than the ones observed in ethene protonation reaction,[22] but a similar trend.

Besides, we can clearly identify three different types of interactions related to the confinement effects: five $O_Z\cdots C$ interactions; four $O_Z\cdots H-C$ interactions; and two $O_{Z2}\cdots H-C$ interactions (the last one involved the bridge Al−O−Si of H-Y). All of these interactions show $d_{X\cdots Y} > 2.4$ Å, and $\rho(r)$ values range from 0.005 to 0.011 au and $\nabla^2\rho(r)$ and $H(r)$ values are positive, showing characteristics of closed-shell interactions, that is, bonds in which ionic interactions are the dominant ones.

In this transition state, $\rho(r)$ values for interactions related to formed/broken bonds are large, whereas those values for interactions related to confinement effects are several but with small values. Thus, the bond-breaking and bond-forming processes represent 87% of total density, while 13% correspond to the confinement effect.

3.2.3. Intermediate 1. The next step involves stabilization through the formation of intermediate like carbenium ion (interm1, Figure 3). The principal interaction related to the stabilization of the carbenium ion is $O_{Z2}\cdots C$ [between the oxygen atom in Si−O−Al bridge and the carbon atom of vinyl moiety]. The topological properties at the $O_{Z2}\cdots C$ BCP [$\rho(r) = 0.0217$ au; $\nabla^2\rho(r) = 0.0715$ au; $H(r) > 0$] are indicative of a closed-shell interaction (weak electrostatic or ionic bond). The $H(r)$ value is positive, which suggests poor electron sharing between guest molecule and the catalyst.

In addition, a large quantity of weak host−guest interactions related to the confinement effects are observed. We found six $O_Z\cdots H-C$ interactions; two $O_Z\cdots C$; 1 $O_Z\cdots\pi CC$, $O_{Z1}\cdots C$; and finally one $O_{Z1}\cdots H_{Z1}-C$. All of these interactions are of electrostatic nature; however, interactions involving oxygen of acid site are stronger than the other ones.

Buurmans et al. found for this intermediate an energy of 2.6 kcal mol^{-1} when van der Waals interactions between the carbocation and the zeolite framework are neglected; however, after correcting for the vdW interactions, the energy decreased to −21.2 kcal mol^{-1}.[20] This suggested the larger contribution of vdW interactions in stabilization of the formed carbenium ion. Our results, based on the identification and quantification of weak host−guest interactions, confirm this observation. We observed by contrast of TS1 that the contributions of weak interactions to the confinement effect are higher than interactions related to the reaction itself (78 vs 22% of total density). The host−guest interactions contribute larger as the organic molecules adopt a conformation, which optimizes the strength of these interactions. In addition, the energy of stabilization is low. Summarizing, the interactions related to the confinement effects contribute significantly to the stabilization of free carbenium ion inside the zeolite cavity.

*3.2.4. Transition State (**TS2**).* In this step, the $O_{Z2}\cdots C$ interaction is stronger than the same one at interm1 [$\rho(r) = 0.0321$ au; $\nabla^2\rho(r) = 0.0934$ au], whereas $H(r)$ is slightly negative. Within the AIM framework, such an interaction is usually considered as closed-shell interaction (ionic interactions) with some degree of covalence; thus, this interaction strengthened in the TS2. This step of the reaction has a very low activation energy, then the carbenium ion is highly reactive giving rise to the alkoxide product in the next step of reaction.

Regarding the confinement effects, the TS2 species has two different O···H−C and O···C bonds, which are characterized by values of $\rho(r)$ that are around 0.003−0.016 au, and all interactions show characteristic of closed-shell interactions. In general, the interactions related to the oxygen O_{Z1} are stronger than the other ones. Similar to the previous step, the contributions of weak interactions to confinement effect are higher than bond forming (69 vs 31%).

3.2.5. Intermediate 2. The formation of $O_{Z2}-C$ bond gives rise to the alkoxide intermediate or interm2, then the major contribution to the stabilization energy should be the one involved in forming this bond.

The $O_{Z2}-C$ distance is shorter than the previous steps (1.52 vs 2.30 Å in TS2 and 2.50 Å in interm1), and the interaction is stronger, as would be expected. In this case, the $\rho(r)$ value is large, $\nabla^2\rho(r) < 0$, and $H(r)$ is negative with a large value, showing characteristic of shared interaction or covalent bond. This intermediate is stabilized by different types of non-covalent interactions as $O_Z\cdots H-C$ [where $\rho(r)$ values range from 0.021 to 0.002 au and $\nabla^2\rho(r)$ and $H(r)$ values are positive], $O_Z\cdots C$ [where $\rho(r)$ values range from 0.010 to 0.002 au], and finally two weak interactions with O_{Z1}.

The main interaction related with the formed adsorbate−catalyst bond signifies 69.2% of total electron density contribution, while only 30.2% corresponds to interactions related to confinement effects, demonstrating that the alkoxide is stabilized via a covalent bond instead of electrostatic interactions.

It is interesting to note that the adsorbate−catalyst bond in alkoxide is weaker than the $C_{ethylene}-O_{zeolite}$ bond observed on protonation of ethylene on an acidic zeolite model.[22] Thus, the intermediate is bound to the catalyst, but due to the steric restriction of aromatic ring or large size of guest molecule, it results in a weaker interaction with the zeolite.

Summing up, our results showed that the number of stabilizing contacts related to confinement effects changes (between 11 and 9) during the reaction. Additionally, not only HB interactions, but also several unusual interactions of different types are found. All of them contribute to stabilize the different steps of the reaction, where numerous O_z atoms of zeolite lattice participate on these bonding interactions. It is demonstrated that energy stabilization by the zeolite lattice related to confinement is particularly important in the free carbenium ion (interm1). Besides, the intermediate 2 has been also shown to be a truly alkoxide species with a C−O bond.

The results also reveal that protonation reaction of styrene catalyzed by zeolites with large cavities are governed by confinement effect. In other words, zeolite confinement effect is a crucial factor that may affect the catalytic activity even on zeolites with large pore size and void structure as H-Y.

3.3. Analysis from RCP and CCPs. As it can be seen in the molecular graphs represented in Figure 3, several bond critical points between the reactant and catalyst give rise to several ring critical points, and consequently, additional cage structures are formed inside the cavity. Considering the analysis of RCP and CCP (Table 2), we arrive at similar conclusions discussed previously.

DOI: 10.1021/acs.jpcc.8b07357
J. Phys. Chem. C 2018, 122, 27350−27359

Table 3. Net Atomic Charges, $q(\Omega)$, Obtained by Integrating the Electron Charge Density over the Atomic Basin (in au)

Ω	H-Y	styrene	free carbenium ion	π-complex	TS1	interm1	TS2	interm2
H_{Z1}	+0.681		+0.041	+0.670	+0.384	+0.093	+0.053	−0.001
O_{Z1}	−1.509			−1.559	−1.614	−1.680	−1.678	−1.682
O_{Z2}	−1.673			−1.678	−1.677	−1.662	−1.626	−1.444
C_1		+0.008	+0.031	−0.016	+0.011	+0.040	+0.036	−0.018
C_2		−0.010	+0.027	−0.017	+0.007	+0.027	+0.030	+0.004
C_3		+0.000	+0.048	+0.016	+0.033	+0.047	+0.043	+0.021
C_4		−0.003	+0.038	+0.012	+0.032	+0.035	+0.031	+0.010
C_5		+0.002	+0.046	+0.023	+0.042	+0.045	+0.040	+0.017
C_6		−0.005	+0.027	−0.004	+0.022	+0.042	+0.037	+0.011
C_7		+0.002	+0.042	−0.034	+0.047	+0.079	+0.090	+0.369
C_8		−0.018	+0.051	−0.063	−0.135	+0.064	+0.067	+0.073
$H(C_2)$		+0.000	+0.066	−0.003	+0.024	+0.051	+0.046	+0.003
$H(C_3)$		+0.005	+0.077	+0.029	+0.050	+0.061	+0.054	+0.026
$H(C_4)$		+0.005	+0.087	+0.028	+0.048	+0.055	+0.042	+0.014
$H(C_5)$		+0.004	+0.079	+0.016	+0.042	+0.045	+0.042	+0.015
$H(C_6)$		+0.001	+0.070	+0.019	+0.053	+0.060	+0.057	+0.029
$H(C_7)$		−0.003	+0.089	+0.033	+0.093	+0.118	+0.121	+0.051
$H(C_8)$		+0.011	+0.090	+0.058	+0.102	+0.064	+0.087	+0.008
$H(C_8)$		+0.001	+0.090	+0.024	+0.047	+0.046	+0.049	+0.053
$\sum q(\Omega)_{\text{organic fragment}}$ [a]		0.000	+0.999	+0.122	+0.902	+0.971	+0.925	+0.682

[a]Total charge of the organic fragment calculated as the sum of the atomic charge in all atoms of organic unit inside the zeolite.

In isolated H-Y zeolite, 44 RCPs are found. When the guest molecule is adsorbed, 22 new RCPs (involving guest molecule and zeolite atoms) and 5 CCPs appear in the π-complex. The $\rho(r)$ values at RCPs range from 0.000001 to 0.005 au. The largest RCP value corresponds to the ring formed through the bond paths between $H_{Z1}\cdots\pi$CC and $O_{Z2}\cdots$H−C interactions together with the O_{Z2}−Al−O_{Z1} skeleton (six-membered ring or −H$\cdots O_{Z2}$−Al−O_{Z1}−$H_Z\cdots\pi$CC). In this case, the RCPs and CCP range is low enough if it is compared to BCPs values, and the $\sum\rho(r)$ value is about 0.1 and 0.01 au for RCPs and CCP, respectively. All species involved in the reaction approximately show similar values. In summary, the presence of RCPs and CCPs provides additional stability to the system. In addition, it is interesting to highlight that the three local minima in the potential energy surface (most stable species) form ring structures in which $\sum\rho(r)$ is about 0.97 au.

3.4. Net Atomic Charges Derived from QTAIM Analysis. If we analyze how the net charge of organic fragment is modified throughout the reaction, then interesting conclusions are found. Net atomic charges, $q(\Omega)$, obtained by integrating the charge density over the atomic basin are given in Table 3.

Through comparing the net charge distribution of isolated styrene molecule with styrene in adsorbed π-complex, it can be found that its electronic structure is subjected to changes upon adsorption. It can be seen in Table 3 that C_7 and C_8 carry the highest negative charges after interacting with H-Y zeolite. The electron density is transferred from the whole guest molecule (the electron pair donor) throughout the zeolite surface (the electron pair acceptor), which results in an increase in the net atomic charge of styrene molecule (from 0 to +0.122e). However, $q(H_{Z1})$ only decreases by 0.01e (from +0681e in isolated H-Y to +0.670 in π-complex) and $q(O_{Z2})$ decreases by 0.05e (from −1.673e to −1.677e); the electron density is transferred to the atoms of zeolite framework involved in the host−guest interactions mentioned above.

We also calculated $\sum q(\Omega)$ in carbocationic fragments, expressed as the sum of net atomic charges including all atoms of carbocationic fragments ($C_8H_9^+$). The total net atomic charge on the $C_8H_9^+$ carbocationic fragment in TS1 is +0.902e, and in interm1, it is about +0.971e (while $\sum q(\Omega)$ in free carbenium ion is +0.999e, see Table 3). Thus, it can be observed that zeolite helps to stabilize the positive charge of carbocationic intermediate.

If we compare interm1 and interm2, then we can observe that the total net atomic charge considered achieves +0.971e and +0.682e, respectively. That is, decrease by 0.29e and the most significant changes are related to atoms involved in O_{Z2}−C bond forming (O_{Z2} and C_7 atoms), showing the stabilization of alkoxide species by the zeolite lattice.

4. CONCLUSIONS

In the present work, we studied the protonation reaction of styrene inside the cavity of acidic H-Y zeolite. Density functional theory calculation using M06-2X functional and analysis of quantum theory of atoms in molecules are used to investigate the confinement effects of zeolite framework on species involved in the reaction. A detailed analysis of the topology of the electron density of interactions among reactants, TS, and intermediate products with the cavity of H-Y zeolite is performed, extracting conclusions about adsorption, catalysis, and confinement effects.

MEPs showed that although the organic molecules are large enough, a large space of the zeolite cavity remains empty, suggesting that confinement effects should not be of paramount importance in this zeolite. However, results from QTAIM analyses showed that the number of stabilizing contacts related to confinement effects are of paramount importance and change during the reaction. Additionally, not only HB interactions but also several unusual interactions of different types are found. All of them contribute to stabilize the different steps of the reaction, where numerous O_z atoms of zeolite lattice participate on these stabilizing interactions. The presence of numerous RCPs and CCPs provides additional stability to the system.

DOI: 10.1021/acs.jpcc.8b07357
J. Phys. Chem. C 2018, 122, 27350−27359

It is demonstrated that energy stabilization by the zeolite lattice related to confinement is particularly important in the free carbenium ion, where only interactions between a fraction of atoms of zeolite lattice under the organic fragment are observed, in contrast to the results obtained from smaller zeolites such as H-β or H-ZM-5. Besides, intermediate 2 has been also shown to be a truly alkoxide species with a C−O bond. Along the reaction coordinate, the electron density is transferred from the whole guest molecule throughout the zeolite surface.

Identification and quantification of weak host−guest interactions between zeolite framework and styryl cation support the larger contribution of closed-shell interactions in stabilization of the formed carbenium ion. Our results clearly show that the reaction energies for all formed species inside a zeolite with large void structure are also significantly governed by the confinement effects related to weak host−guest interactions. In other words, zeolite confinement effect is a crucial factor that may affect the catalytic activity even on zeolites with large pore size and void structure as H-Y.

■ ASSOCIATED CONTENT

Supporting Information

The Supporting Information is available free of charge on the ACS Publications website at DOI: 10.1021/acs.jpcc.8b07357.

Isosurface plots of reduced density gradient (Figure S1) (PDF)

■ AUTHOR INFORMATION

Corresponding Author

*E-mail: mfzalazar@conicet.gov.ar.

ORCID

M. Fernanda Zalazar: 0000-0003-0316-7159

Notes

The authors declare no competing financial interest.

■ ACKNOWLEDGMENTS

The authors acknowledge Agencia Nacional de Promoción Científica y Tecnológica (grant FONCYT-PICT-0465), Secretaría General de Ciencia y Técnica de la Universidad Nacional del Nordeste (grant F017-2014, SGCyT-UNNE), and Consejo Nacional de Investigaciones Científicas y Técnicas (grant PIP-0678 CONICET) of Argentina for financial support. They also acknowledge the use of CPUs from the High Performance Computing Center of the Northeastern of Argentina (CECONEA).

■ REFERENCES

(1) Climent, M. J.; Corma, A.; Iborra, S. Zeolites as Catalysts for the Synthesis of Fine Chemicals. In *Zeolites and Catalysis: Synthesis, Reactions and Applications*; Čejka, J., Corma, A., Zones, S., Eds.; Wiley-VCH Verlag GmbH & Co. KGaA: Weinheim, 2010.

(2) Primo, A.; Garcia, H. Zeolites as Catalysts in Oil Refining. *Chem. Soc. Rev.* **2014**, *43*, 7548−7561.

(3) Corma, A. State of the Art and Future Challenges of Zeolites as Catalysts. *J. Catal.* **2003**, *216*, 298−312.

(4) Chu, Y.; Han, B.; Zheng, A.; Deng, F. Influence of Acid Strength and Confinement Effect on the Ethylene Dimerization Reaction over Solid Acid Catalysts: A Theoretical Calculation Study. *J. Phys. Chem. C* **2012**, *116*, 12687−12695.

(5) Derouane, E. G. Zeolites as Solid Solvents. *J. Mol. Catal. A: Chem.* **1998**, *134*, 29−45.

(6) Sastre, G.; Corma, A. The Confinement Effect in Zeolites. *J. Mol. Catal. A: Chem.* **2009**, *305*, 3−7.

(7) Gounder, R.; Iglesia, E. The Catalytic Diversity of Zeolites: Confinement and Solvation Effects within Voids of Molecular Dimensions. *Chem. Commun.* **2013**, *49*, 3491−3509.

(8) Li, X.; Sun, Q.; Li, Y.; Wang, N.; Lu, J.; Yu, J. Confinement Effect of Zeolite Cavities on Methanol-to-Olefin Conversion: A Density Functional Theory Study. *J. Phys. Chem. C* **2014**, *118*, 24935−24940.

(9) Mazar, M. N.; Al-Hashimi, S.; Bhan, A.; Cococcioni, M. Methylation of Ethene by Surface Methoxides: A Periodic PBE + D Study across Zeolites. *J. Phys. Chem. C* **2012**, *116*, 19385−19395.

(10) De Moor, B. A.; Reyniers, M.-F.; Gobin, O. C.; Lercher, J. A.; Marin, G. B. Adsorption of C2−C8 n-Alkanes in Zeolites. *J. Phys. Chem. C* **2011**, *115*, 1204−1219.

(11) Sacchetto, V.; Bisio, C.; Olivas Olivera, D. F.; Paul, G.; Gatti, G.; Braschi, I.; Berlier, G.; Cossi, M.; Marchese, L. Interactions of Toluene and n-Hexane on High Silica Zeolites: An Experimental and Computational Model Study. *J. Phys. Chem. C* **2015**, *119*, 24875−24886.

(12) Resasco, D. E.; Wang, B.; Crossley, S. Zeolite-Catalysed C−C Bond Forming Reactions for Biomass Conversion to Fuels and Chemicals. *Catal. Sci. Technol.* **2016**, *6*, 2543−2559.

(13) Sastre, G. Confinement Effects in Methanol to Olefins Catalysed by Zeolites: A Computational Review. *Front. Chem. Sci. Eng.* **2016**, *10*, 76−89.

(14) Shen, W. A Theoretical Study of Confinement Effect of Zeolite on the Ethylene Dimerization Reaction. *Microporous Mesoporous Mater.* **2017**, *247*, 136−144.

(15) Hemelsoet, K.; Nollet, A.; Vandichel, M.; Lesthaeghe, D.; Van Speybroeck, V.; Waroquier, M. The Effect of Confined Space on the Growth of Naphthalenic Species in a Chabazite-Type Catalyst: A Molecular Modeling Study. *ChemCatChem* **2009**, *1*, 373−378.

(16) Jones, A. J.; Zones, S. I.; Iglesia, E. Implications of Transition State Confinement within Small Voids for Acid Catalysis. *J. Phys. Chem. C* **2014**, *118*, 17787−17800.

(17) Li, J.; Wei, Y.; Chen, J.; Xu, S.; Tian, P.; Yang, X.; Li, B.; Wang, J.; Liu, Z. Cavity Controls the Selectivity: Insights of Confinement Effects on MTO Reaction. *ACS Catal.* **2015**, *5*, 661−665.

(18) Fu, J.; Feng, X.; Liu, Y.; Yang, C. Effect of Pore Confinement on the Adsorption of Mono-Branched Alkanes of Naphtha in ZSM-5 and Y Zeolites. *Appl. Surf. Sci.* **2017**, *423*, 131−138.

(19) Song, B.; Chu, Y.; Li, G.; Wang, J.; Lo, A.-Y.; Zheng, A.; Deng, F. Origin of Zeolite Confinement Revisited by Energy Decomposition Analysis. *J. Phys. Chem. C* **2016**, *120*, 27349−27363.

(20) Buurmans, I. L. C.; Pidko, E. A.; de Groot, J. M.; Stavitski, E.; van Santen, R. A.; Weckhuysen, B. M. Styrene Oligomerization as a Molecular Probe Reaction for Zeolite Acidity: A UV-Vis Spectroscopy and DFT Study. *Phys. Chem. Chem. Phys.* **2010**, *12*, 7032−7040.

(21) Ristanović, Z.; Kubarev, A. V.; Hofkens, J.; Roeffaers, M. B. J.; Weckhuysen, B. M. Single Molecule Nanospectroscopy Visualizes Proton-Transfer Processes within a Zeolite Crystal. *J. Am. Chem. Soc.* **2016**, *138*, 13586−13596.

(22) Zalazar, M. F.; Peruchena, N. M. Topological Analysis of the Electronic Charge Density in the Ethene Protonation Reaction Catalyzed by Acidic Zeolite. *J. Phys. Chem. A* **2007**, *111*, 7848−7859.

(23) Zalazar, M. F.; Peruchena, N. M. Topological Description of the Bond Breaking and Bond Forming Processes of the Alkene Protonation Reaction in the Zeolite Chemistry: An AIM Study. *J. Mol. Model.* **2011**, *17*, 2501−2511.

(24) Zalazar, M. F.; Peruchena, N. Laplacian of the Electron Density: A Hole-Lump Interaction as a Tool to Study Stereo-electronic Control of Chemical Reactions. *J. Phys. Org. Chem.* **2014**, *27*, 327−335.

(25) Zalazar, M. F.; Duarte, D. J. R.; Peruchena, N. M. Adsorption of Alkenes on Acidic Zeolites. Theoretical Study Based on the Electron Charge Density. *J. Phys. Chem. A* **2009**, *113*, 13797−13807.

(26) Parravicini, O.; Bogado, M. L.; Rojas, S.; Angelina, E. L.; Andujar, S. A.; Gutierrez, L. J.; Cabedo, N.; Sanz, M. J.; López-Gresa,

M. P.; Cortes, D.; Enriz, R. D. Tetrahydroisoquinolines Functionalized with Carbamates as Selective Ligands of D2 Dopamine Receptor. *J. Mol. Model.* **2017**, *23*, 273.
(27) Zalazar, M. F.; Paredes, E. N.; Romero Ojeda, G. D.; Cabral, N. D.; Peruchena, N. Study of Confinement and Catalysis Effects of the Reaction of Methylation of Benzene by Methanol in H-Beta and H-ZSM-5 Zeolites by Topological Analysis of Electron Density. *J. Phys. Chem. C* **2018**, *122*, 3350−3362.
(28) Higgins, J. B. Chapter 2 Large Pore Zeolite Frameworks and Materials. *Catal. Today* **1994**, *19*, 7−26.
(29) Serra, J. M.; Corma, A.; Farrusseng, D.; Baumes, L.; Mirodatos, C.; Flego, C.; Perego, C. Styrene from Toluene by Combinatorial Catalysis. *Catal. Today* **2003**, *81*, 425−436.
(30) Valencia, D. Elucidating the Structure of Light Absorbing Styrene Carbocation Species Formed within Zeolites. *Phys. Chem. Chem. Phys.* **2017**, *19*, 15050−15058.
(31) Corma, A.; Garcia, H. A Unified Approach to Zeolites as Acid Catalysts and as Supramolecular Hosts Exemplified. *J. Chem. Soc., Dalton Trans.* **2000**, 1381−1394.
(32) Cozens, F. L.; Bogdanova, R.; Régimbald, M.; García, H.; Martí, V.; Scaiano, J. C. Photochemical and Thermal Behavior of Styrenes within Acidic and Nonacidic Zeolites. Radical Cation Versus Carbocation Formation. *J. Phys. Chem. B* **1997**, *101*, 6921−6928.
(33) Bader, R. F. W. *Atoms in Molecules. A Quantum Theory*; Oxford Science Publications: London, 1990.
(34) Popelier, P. L. A. *Atoms in Molecules. An Introduction*; Pearson Education: Harlow, U.K., 2000.
(35) Baerlocher, C.; McCusker, L. B. *Database of Zeolite Structures*. http://www.iza-structure.org/databases/.
(36) Fang, H.; Zheng, A.; Xu, J.; Li, S.; Chu, Y.; Chen, L.; Deng, F. Theoretical Investigation of the Effects of the Zeolite Framework on the Stability of Carbenium Ions. *J. Phys. Chem. C* **2011**, *115*, 7429−7439.
(37) Zhao, Y.; Truhlar, D. G. The Minnesota Density Functionals and Their Applications to Problems in Mineralogy and Geochemistry. *Rev. Mineral. Geochem.* **2010**, *71*, 19−37.
(38) Zhao, Y.; Truhlar, D. G. Benchmark Data for Interactions in Zeolite Model Complexes and their Use for Assessment and Validation of Electronic Structure Methods. *J. Phys. Chem. C* **2008**, *112*, 6860−6868.
(39) Maihom, T.; Boekfa, B.; Sirijaraensre, J.; Nanok, T.; Probst, M.; Limtrakul, J. Reaction Mechanisms of the Methylation of Ethene with Methanol and Dimethyl Ether over H-ZSM-5: An ONIOM Study. *J. Phys. Chem. C* **2009**, *113*, 6654−6662.
(40) Kongpatpanich, K.; Nanok, T.; Boekfa, B.; Probst, M.; Limtrakul, J. Structures and Reaction Mechanisms of Glycerol Dehydration over H-ZSM-5 Zeolite: A Density Functional Theory Study. *Phys. Chem. Chem. Phys.* **2011**, *13*, 6462−6470.
(41) Maihom, T.; Pantu, P.; Tachakritikul, C.; Probst, M.; Limtrakul, J. Effect of the Zeolite Nanocavity on the Reaction Mechanism of n-Hexane Cracking: A Density Functional Theory Study. *J. Phys. Chem. C* **2010**, *114*, 7850−7856.
(42) Charoenwiangnuea, P.; Maihom, T.; Kongpracha, P.; Sirijaraensre, J.; Limtrakul, J. Adsorption and Decarbonylation of Furfural over H-ZSM-5 Zeolite: A DFT Study. *RSC Adv.* **2016**, *6*, No. 105888.
(43) Gomes, J.; Zimmerman, P. M.; Head-Gordon, M.; Bell, A. T. Accurate Prediction of Hydrocarbon Interactions with Zeolites Utilizing Improved Exchange-Correlation Functionals and QM/MM Methods: Benchmark Calculations of Adsorption Enthalpies and Application to Ethene Methylation by Methanol. *J. Phys. Chem. C* **2012**, *116*, 15406−15414.
(44) Gomes, G. J.; Zalazar, M. F.; Lindino, C. A.; Scremin, F. R.; Bittencourt, P. R. S.; Costa, M. B.; Peruchena, N. M. Adsorption of Acetic Acid and Methanol on H-Beta Zeolite: An Experimental and Theoretical Study. *Microporous Mesoporous Mater.* **2017**, *252*, 17−28.
(45) Stewart, J. J. P. Optimization of Parameters for Semiempirical Methods V: Modification of NDDO Approximations and Application to 70 Elements. *J. Mol. Model.* **2007**, *13*, 1173−1213.
(46) Däumer, D.; Räuchle, K.; Reschetilowski, W. Experimental and Computational Investigations of the Deactivation of H-ZSM-5 Zeolite by Coking in the Conversion of Ethanol into Hydrocarbons. *ChemCatChem* **2012**, *4*, 802−814.
(47) Soscún, H.; Hernández, J.; Castellano, O.; Arrieta, F.; Ruette, F.; Sierralta, A.; Machado, F.; Rosa-Brusin, M. The Interaction of *Cis*-2-Butene over a 10-Ring Brønsted Acid Site of Zeolite: A Theoretical Study. *J. Mol. Catal. A: Chem.* **2003**, *192*, 63−72.
(48) Uzunova, E. L.; Mikosch, H.; St. Nikolov, G. Density Functional Study of Copper-Exchanged Zeolites and Related Microporous Materials: Adsorption of Nitrosyls. *Int. J. Quantum Chem.* **2013**, *113*, 723−728.
(49) Frisch, M. J., Trucks, G. W.; Schlegel, H. B.; Scuseria, G. E.; Robb, M. A.; Cheeseman, J. R.; Montgomery, J. A.; Vreven, T.; Kudin, K. N.; Burant, J. C. et al. *Gaussian 09*, revision A.01; Gaussian, Inc.: Wallingford, CT, 2009.
(50) Matta, C. F.; Boyd, R. J. *The Quantum Theory of Atoms in Molecules: From Solid State to DNA and Drug Design*; Wiley-VCH: Weinheim, 2007.
(51) Bader, R. F. W. A Bond Path: A Universal Indicator of Bonded Interactions. *J. Phys. Chem. A* **1998**, *102*, 7314−7323.
(52) Keith, T. A. *AIMAll*, version 13.05.06; TK Gristmill Software: Overland Park, KS, 2013.
(53) Johnson, E. R.; Keinan, S.; Mori-Sánchez, P.; Contreras-García, J.; Cohen, A. J.; Yang, W. Revealing Noncovalent Interactions. *J. Am. Chem. Soc.* **2010**, *132*, 6498−6506.
(54) Lu, T.; Chen, F. Multiwfn: A Multifunctional Wavefunction Analyzer. *J. Comput. Chem.* **2012**, *33*, 580−592.
(55) Zhang, W.; Chu, Y.; Wei, Y.; Yi, X.; Xu, S.; Huang, J.; Zhang, M.; Zheng, A.; Deng, F.; Liu, Z. Influences of the Confinement Effect and Acid Strength of Zeolite on the Mechanisms of Methanol-to-Olefins Conversion over H-ZSM-5: A Theoretical Study of Alkenes-Based Cycle. *Microporous Mesoporous Mater.* **2016**, *231*, 216−229.
(56) Chu, Y.; Sun, X.; Yi, X.; Ding, L.; Zheng, A.; Deng, F. Slight Channel Difference Influences the Reaction Pathway of Methanol-to-Olefins Conversion over Acidic H-ZSM-22 and H-ZSM-12 Zeolites. *Catal. Sci. Technol.* **2015**, *5*, 3507−3517.
(57) Van Speybroeck, V.; Hemelsoet, K.; Joos, L.; Waroquier, M.; Bell, R. G.; Catlow, C. R. A. Advances in Theory and their Application within the Field of Zeolite Chemistry. *Chem. Soc. Rev.* **2015**, *44*, 7044−7111.
(58) Arnold, W. D.; Oldfield, E. The Chemical Nature of Hydrogen Bonding in Proteins Via NMR: J-Couplings, Chemical Shifts, and AIM Theory. *J. Am. Chem. Soc.* **2000**, *122*, 12835−12841.
(59) Cremer, D.; Kraka, E. A Description of the Chemical Bond in Terms of Local Properties of the Electron Density and Energy. *Croat. Chem. Acta* **1984**, *57*, 1259−1281.
(60) Jenkins, S.; Morrison, I. The Chemical Character of the Intermolecular Bonds of Seven Phases of Ice as Revealed by Ab Initio Calculation of Electron Densities. *Chem. Phys. Lett.* **2000**, *317*, 97−102.

DOI: 10.1021/acs.jpcc.8b07357
J. Phys. Chem. C 2018, 122, 27350−27359